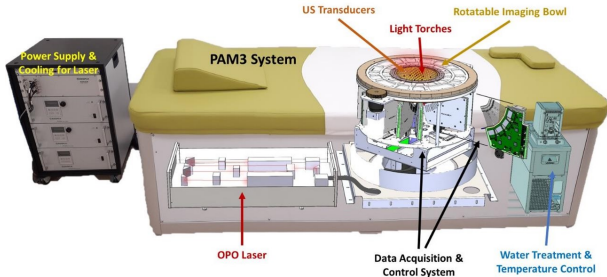


Ultrasonic Breast Tomography via 3D Full Waveform Inversion

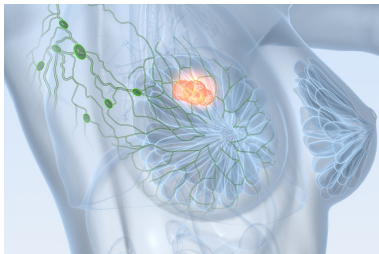
Felix Lucka (he/him/his) & the PAMMOTH team



Motivation: Breast Cancer Imaging

Most common cause of cancer death in women worldwide.

- 25% of all cancer cases in women
- 15% of all cancer deaths in women

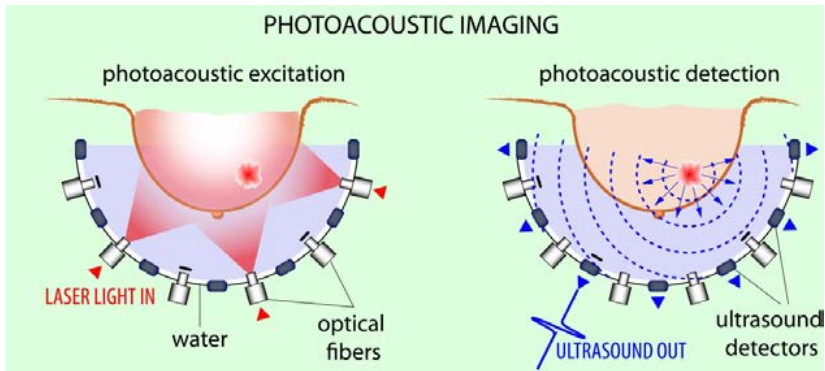


Despite advances in early detection and diagnosis:

Urgent need for novel imaging techniques providing higher specificity, contrast and image resolution than X-ray mammography at lower costs than MRI.

Quantitative Photoacoustic Breast Imaging

- hybrid imaging: "light in, sound out"
- non-ionizing, near-infrared radiation
- quantitative images of optical properties
- novel diagnostic information

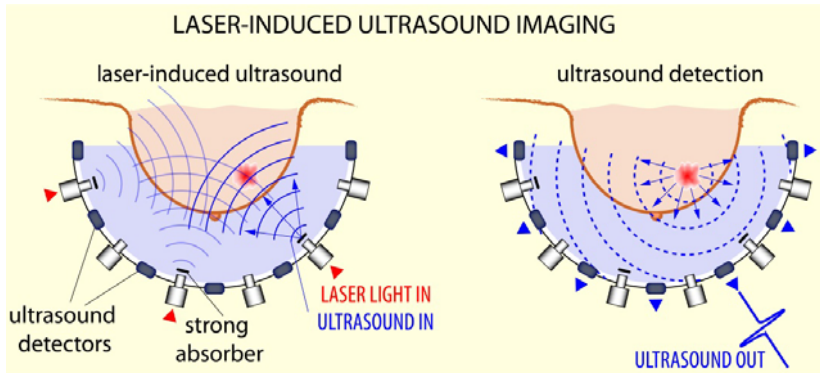


Photoacoustic Imaging: Spectral Properties

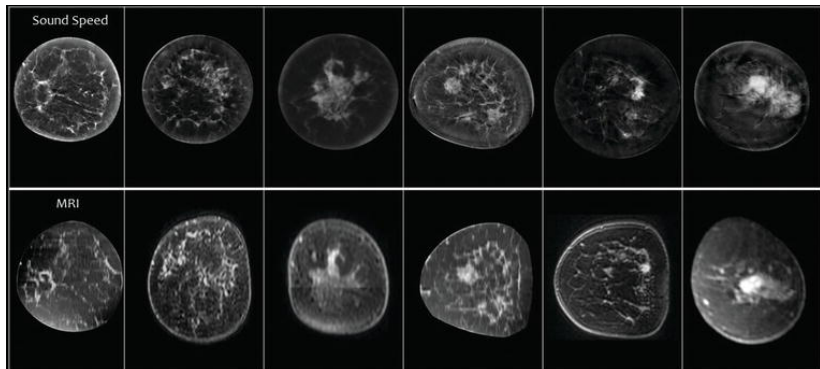
- different wavelengths allow quantitative spectroscopic examinations.
- gap between oxygenated and deoxygenated blood.

Quantitative Ultrasonic Breast Imaging

- "sound in, sound out"
- different from conventional US but as safe
- quantitative images of acoustic properties
- novel diagnostic information



Speed of Sound vs MRI Images

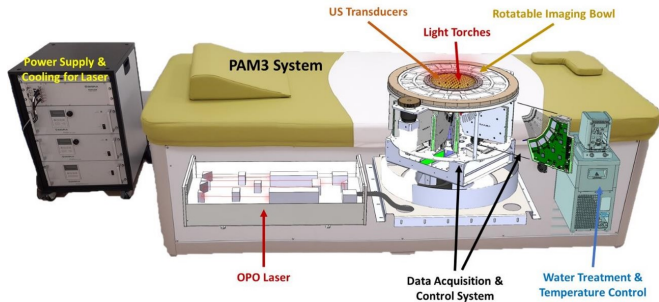


Taken from:



Duric, Littrup, 2017. Breast Ultrasound Tomography, *IntechOpen*.

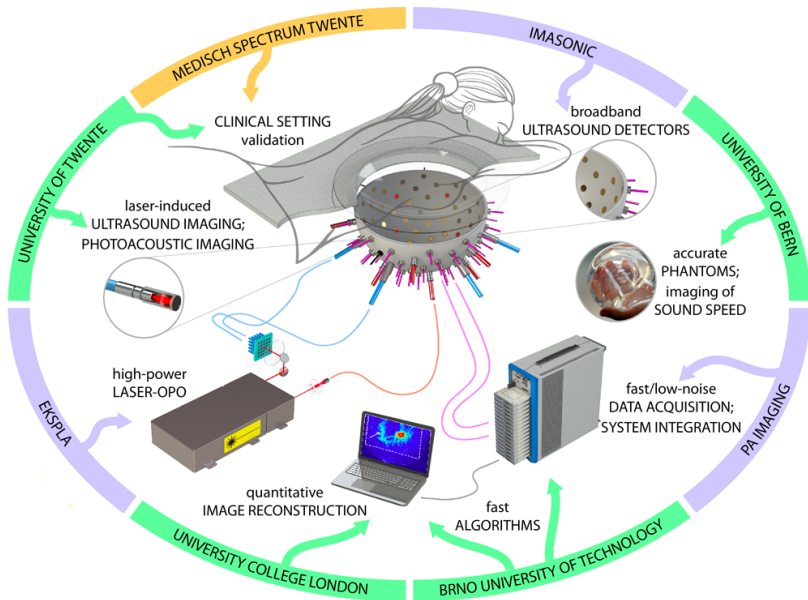
Photoacoustic and Ultrasonic Mammography Scanner



Aim: novel diagnostic information from high resolution maps of optical and acoustic properties

- 512 US transducers on rotatable half-sphere
- 40 optical fibers for photoacoustic excitation
- fully 3D, isotropic resolution $\leq 0.5\text{mm}$
- ! optimized for photoacoustic imaging

The PAMMOTH Team



simulation studies for

- ultrasonic transducer specification
- light excitation design
- sensing pattern design
- measurement protocol design

reconstruction algorithm design:

- accuracy vs. computational time/resources/complexity
- scanner modelling
- assist high performance computing implementation

assist **phantom & calibration design**

process data, refine measurement procedures

Ultrasound Tomography Reconstruction Approaches

$$(c(x)^{-2}\partial_t^2 - \Delta)p_i(x, t) = s_i(x, t), \quad f_i = M_i p_i \quad i = 1, \dots, n_{src}$$

Travel time tomography: geometrical optics approximation.

- ✓ robust & computationally efficient
- ! valid for high frequencies (attenuation!), low res, lots of data



Javaherian, L, Cox, 2020. Refraction-corrected ray-based inversion for three-dimensional ultrasound tomography of the breast, *Inverse Problems*.

Full waveform inversion (FWI): fit full wave model to all data.

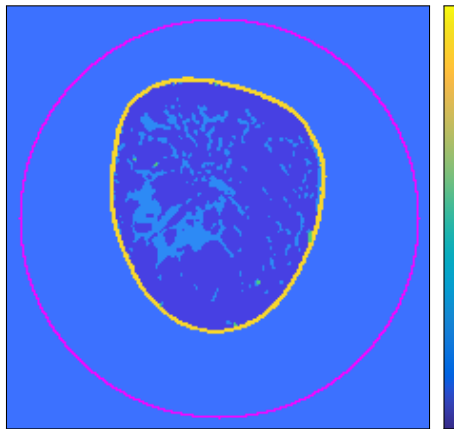
- ✓ high res from little data, transducer modelling, constraints
- ! many wave simulations, complex numerical optimization
- low TRL but already used in 2D systems



Pérez-Liva, Herraiz, Udías, Miller, Cox, Treeby 2017. Time domain reconstruction of sound speed and attenuation in ultrasound computed tomography using full wave inversion, *JASA*.

FWI Illustration in 2D

SOS ground truth c^{true}

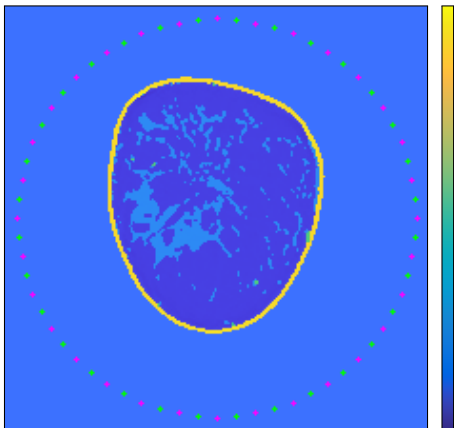


color range 1450 - 1670 m/s

- 1mm resolution
- 222^2 voxel
- 836 voxels on surface (pink)
- TTT would need 836^2 source-receiver combos for high res result

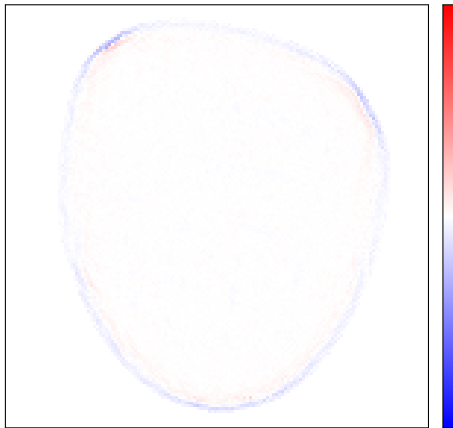
FWI Illustration in 2D: 32 Sensors, 32 Receivers

SOS reconstruction c^{rec}



color range 1450 - 1670 m/s

reconstruction error $c^{true} - c^{rec}$



color range -50 - 50 m/s

3D Time Domain FWI for Breast UST

$$\min_{c \in \mathcal{C}} \sum_i^{n_{src}} \mathcal{D}(M_i A^{-1}(c) s_i, f_i^\delta)$$
$$\nabla_c \mathcal{D}(f(c), f^\delta) = 2 \int_0^T \frac{1}{c(x)^3} \left(\frac{\partial^2 p(x, t)}{\partial t^2} \right) q^*(x, t)$$

Challenges and solutions for 3D:

- ! $2 \times n_{src}$ wave simulations per gradient
- ! computationally & stochastically efficient gradient estimator
- ! memory requirements of gradient computation
- ! slow convergence and local minima
- ! computational resources

3D Time Domain FWI for Breast UST

$$\min_{c \in \mathcal{C}} \sum_i^{n_{src}} \mathcal{D}(M_i A^{-1}(c) s_i, f_i^\delta)$$
$$\nabla_c \mathcal{D}(f(c), f^\delta) = 2 \int_0^T \frac{1}{c(x)^3} \left(\frac{\partial^2 p(x, t)}{\partial t^2} \right) q^*(x, t)$$

Challenges and solutions for 3D:

- ! $2 \times n_{src}$ wave simulations per gradient
→ **stochastic quasi-newton optimization (SL-BFGS)**
- ! computationally & stochastically efficient gradient estimator
- ! memory requirements of gradient computation
- ! slow convergence and local minima
- ! computational resources

3D Time Domain FWI for Breast UST

$$\min_{c \in \mathcal{C}} \sum_i^{n_{src}} \mathcal{D}(M_i A^{-1}(c) s_i, f_i^\delta)$$
$$\nabla_c \mathcal{D}(f(c), f^\delta) = 2 \int_0^T \frac{1}{c(x)^3} \left(\frac{\partial^2 p(x, t)}{\partial t^2} \right) q^*(x, t)$$

Challenges and solutions for 3D:

- ! $2 \times n_{src}$ wave simulations per gradient
→ **stochastic quasi-newton optimization (SL-BFGS)**
- ! computationally & stochastically efficient gradient estimator
→ **source encoding for time-invariant systems**
- ! memory requirements of gradient computation
- ! slow convergence and local minima
- ! computational resources

3D Time Domain FWI for Breast UST

$$\min_{c \in \mathcal{C}} \sum_i^{n_{src}} \mathcal{D}(M_i A^{-1}(c) s_i, f_i^\delta)$$
$$\nabla_c \mathcal{D}(f(c), f^\delta) = 2 \int_0^T \frac{1}{c(x)^3} \left(\frac{\partial^2 p(x, t)}{\partial t^2} \right) q^*(x, t)$$

Challenges and solutions for 3D:

- ! $2 \times n_{src}$ wave simulations per gradient
→ **stochastic quasi-newton optimization (SL-BFGS)**
- ! computationally & stochastically efficient gradient estimator
→ **source encoding for time-invariant systems**
- ! memory requirements of gradient computation
→ **time-reversal based gradient computation**
- ! slow convergence and local minima

- ! computational resources

3D Time Domain FWI for Breast UST

$$\min_{c \in \mathcal{C}} \sum_i^{n_{src}} \mathcal{D}(M_i A^{-1}(c) s_i, f_i^\delta)$$
$$\nabla_c \mathcal{D}(f(c), f^\delta) = 2 \int_0^T \frac{1}{c(x)^3} \left(\frac{\partial^2 p(x, t)}{\partial t^2} \right) q^*(x, t)$$

Challenges and solutions for 3D:

- ! $2 \times n_{src}$ wave simulations per gradient
→ **stochastic quasi-newton optimization (SL-BFGS)**
- ! computationally & stochastically efficient gradient estimator
→ **source encoding for time-invariant systems**
- ! memory requirements of gradient computation
→ **time-reversal based gradient computation**
- ! slow convergence and local minima
→ **coarse-to-fine multigrid schemes**
- ! computational resources

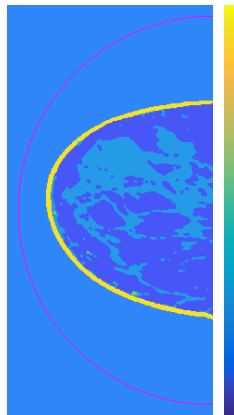
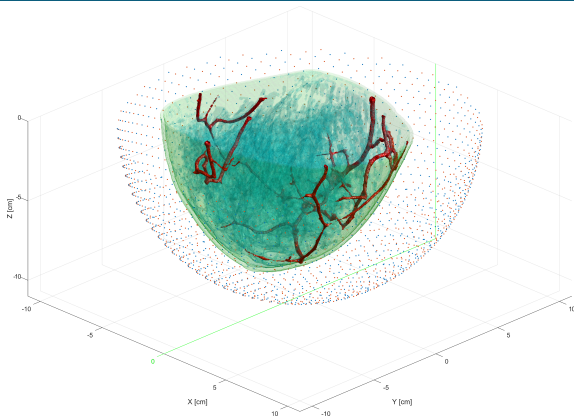
3D Time Domain FWI for Breast UST

$$\min_{c \in \mathcal{C}} \sum_i^{n_{src}} \mathcal{D}(M_i A^{-1}(c) s_i, f_i^\delta)$$
$$\nabla_c \mathcal{D}(f(c), f^\delta) = 2 \int_0^T \frac{1}{c(x)^3} \left(\frac{\partial^2 p(x, t)}{\partial t^2} \right) q^*(x, t)$$

Challenges and solutions for 3D:

- ! $2 \times n_{src}$ wave simulations per gradient
→ **stochastic quasi-newton optimization (SL-BFGS)**
- ! computationally & stochastically efficient gradient estimator
→ **source encoding for time-invariant systems**
- ! memory requirements of gradient computation
→ **time-reversal based gradient computation**
- ! slow convergence and local minima
→ **coarse-to-fine multigrid schemes**
- ! computational resources
→ **runs on single GPU, can utilize multiple GPUs**

3D FWI: Setup

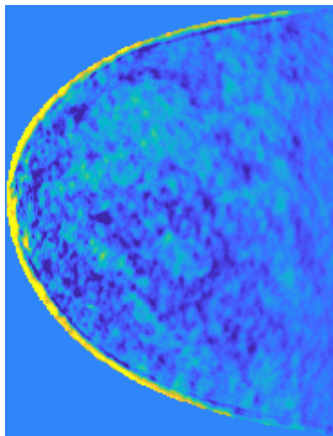


- color range 1435-1665 m/s
- 3D breast phantom at 0.5mm resolution, 1024 sources and receivers
- $442 \times 442 \times 222$ voxel, 3912 time steps

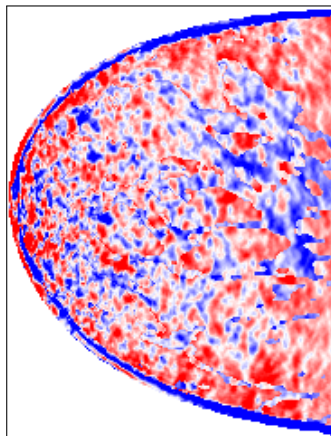


Yang Lou et al. Generation of anatomically realistic numerical phantoms for photoacoustic and ultrasonic breast imaging, *JBO*, 2017.

Starting point in 24h on desktop with single GPU



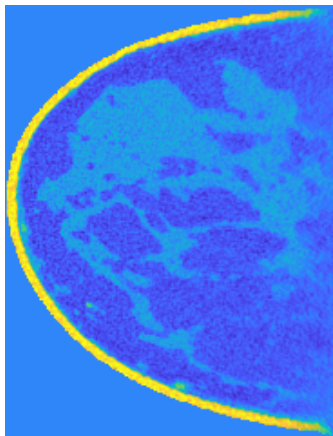
color range 1435 to 1665 m/s



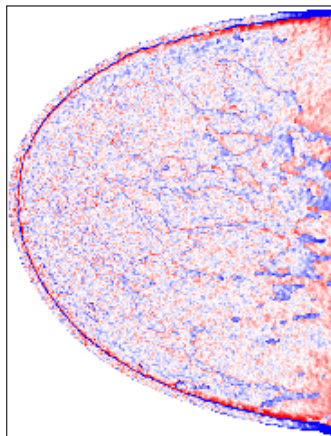
color range -50 to +50 m/s

- single grid
- SGD
- normal single source gradient estimator

3D FWI in 24h on desktop with single GPU



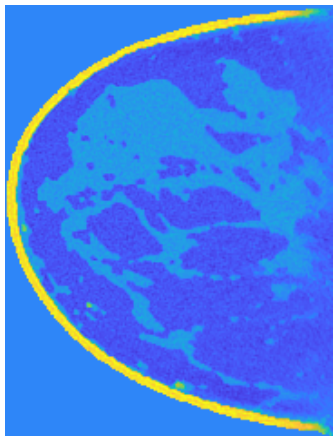
color range 1435 to 1665 m/s



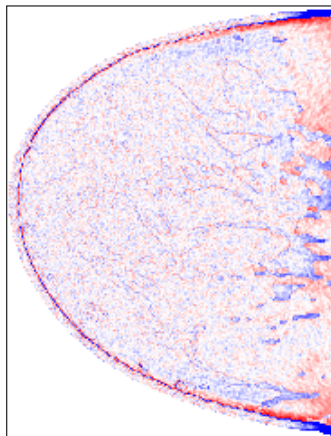
color range -50 to +50 m/s

- multi-grid with 3 level, coarsening factor 2
- SL-BFGS, slowness transform, prog. iter averaging
- time-reversal based source encoding gradient estimator

3D FWI in 24h on cluster with 4 GPU



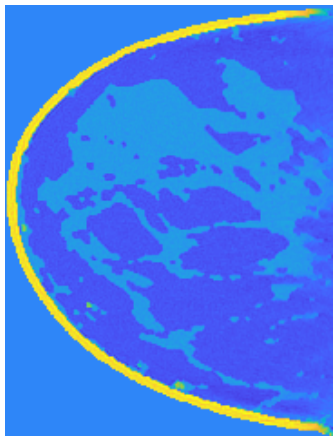
color range 1435 to 1665 m/s



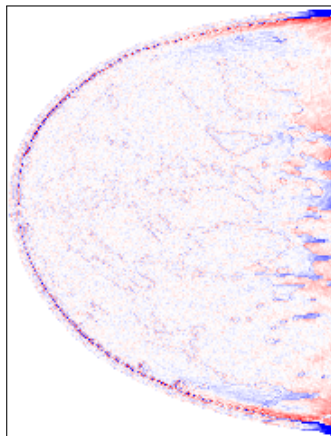
color range -50 to +50 m/s

- multi-grid with 3 level, coarsening factor 2
- SL-BFGS, slowness transform, prog. iter averaging
- time-reversal based source encoding gradient estimator

3D FWI in 24h on cluster with 16 GPU



color range 1435 to 1665 m/s



color range -50 to +50 m/s

- multi-grid with 3 level, coarsening factor 2
- SL-BFGS, slowness transform, prog. iter averaging
- time-reversal based source encoding gradient estimator

FWI for Experimental Data: Where Are We?

- ✓ data from phantom objects, volunteers & patients
- ✓ ray-based SOS reconstructions
- ✓ photoacoustic reconstructions → data pre-processing, scanner & transducer modelling, wave simulations
- ✓ modeling of US protocol, data read-in & pre-processing
- ! model calibration
- ! FWI of phantom objects, quantitative evaluation
- ! FWI of volunteer data
- ! clinical evaluation

- need for novel breast imaging techniques
- photoacoustic (PAT) and ultrasound tomography (UST) give access to high-quality images of optical and acoustic tissue properties
- combined PAT+UST scanner designed & build
- evaluation on data from phantoms, volunteers & patients
- proof-of-concept studies of TD-FWI for high resolution 3D UST
- realization of FWI for experimental data on the way

The CWI logo consists of the letters 'CWI' in white, bold, sans-serif font, set against a red trapezoidal background that tapers to the right.The UCL logo features a white silhouette of a building with a dome, followed by the letters 'UCL' in a large, white, bold, sans-serif font, all on a black rectangular background.

Thank you for your attention!



L, Pérez-Liva, Treeby, Cox, 2021. High Resolution 3D Ultrasonic Breast Imaging by Time-Domain Full Waveform Inversion, *Inverse Problems* 38(2).



PHOTONICS PUBLIC PRIVATE PARTNERSHIP

The Photonics 21 logo features three colored dots (red, green, blue) above the text 'PHOTONICS²¹' in a sans-serif font.The EPSRC logo consists of the letters 'EPSRC' in a large, bold, purple sans-serif font, with a horizontal line above and below the text.

Engineering and Physical Sciences
Research Council



Challenges of High-Resolution FWI in 3D

$$\min_{c \in \mathcal{C}} \sum_i^{n_{src}} \mathcal{D}(f_i(c), f_i^\delta) \quad \text{s.t.} \quad f_i(c) = M_i A^{-1}(c) s_i$$
$$\nabla_c \mathcal{D}(f(c), f^\delta) = 2 \int_0^T \frac{1}{c(x)^3} \left(\frac{\partial^2 p(x, t)}{\partial t^2} \right) q^*(x, t)$$

PAMMOTH scanner example:

- 0.5mm res: comp grid $560 \times 560 \times 300$ voxel = 94M, ROI = 7M
- 1024 transducers, 4000 time samples (multiple sources);

Gradient computation:

- 1 wave sim: ~ 30 min.
- ! **2 wave sim per source**, $n_{src} = 1024 \rightarrow 20$ days per gradient.
stochastic gradient methods $\rightarrow 60$ min per gradient
- ! **storage of forward field** in ROI: ~ 200 GB.
time-reversal based gradient computation $\rightarrow 5 - 25$ GB.

Stochastic Gradient Optimization

$$\mathcal{J} := n_{src}^{-1} \sum_i^{n_{src}} \mathcal{D}_i(c) := n_{src}^{-1} \sum_i^{n_{src}} \mathcal{D}(M_i A^{-1}(c) s_i, f_i^\delta)$$

approx $\nabla \mathcal{J}$ by $|\mathcal{S}|^{-1} \sum_{j \in \mathcal{S}} \nabla \mathcal{D}_j(c)$, $\mathcal{S} \subset \{1, \dots, n_{src}\}$ predetermined.

→ **incremental gradient, ordered sub-set methods**

Instance of **finite sum minimization** similar to **training in machine learning**. Use **stochastic gradient descent (SGD)**:

- momentum, gradient/iterate averaging (SAV, SAGA), variance reduction (SVRG), choice of step size, mini-batch size
- include non-smooth regularizers (SPDHG, SADMM)
- quasi-Newton-type methods, e.g., **stochastic L-BFGS**

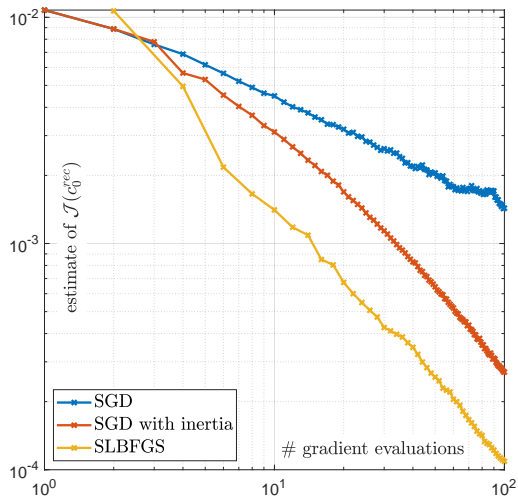


Bottou, Curtis, Nocedal. Optimization Methods for Large-Scale Machine Learning, *arXiv:1606.04838*.



Fabien-Ouellet, Gloaguen, Giroux, 2017. A stochastic L-BFGS approach for full-waveform inversion, *SEG*.

Stochastic Gradient Optimization



Gradient Estimates: Sub-Sampling vs Source Encoding

Computationally & stochastically efficient gradient estimator?

Source Encoding for linear PDE constraints:

$$\text{Let } \hat{s} := \sum_i^{n_{srt}} w_i s_i, \quad \hat{f}^\delta := \sum_i^{n_{srt}} w_i f_i^\delta, \quad \text{with } \mathbb{E}[w] = 0, \text{Cov}[w] = I,$$

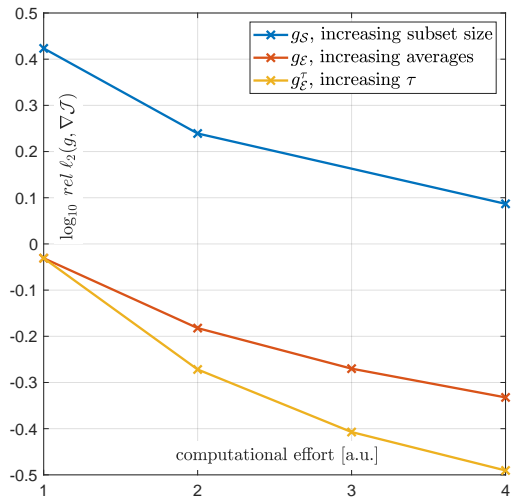
$$\text{then } \mathbb{E} \left[\nabla \left\| MA^{-1}(c) \hat{s} - \hat{f}^\delta \right\|_2^2 \right] = \nabla \sum_i^{n_{src}} \left\| MA^{-1}(c) s_i - f_i^\delta \right\|_2^2$$

- related to covariance trace estimators
- Rademacher distribution ($w_i = \pm 1$ with equal prob)
- add time-shifting for time-invariant PDEs \rightarrow variance control
- can be turned into scanning strategy

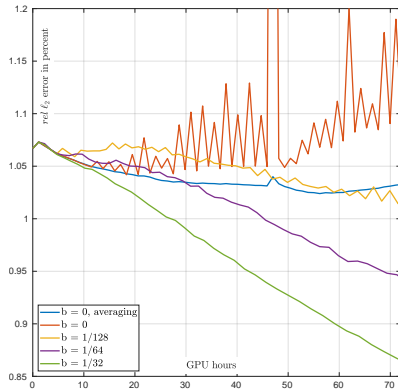
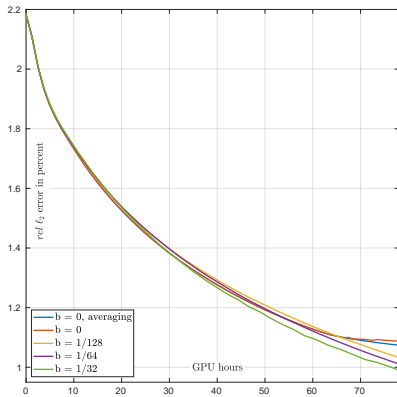


Haber, Chung, Herrmann, 2012. An effective method for parameter estimation with PDE constraints with multiple right-hand sides, *SIAM J. Optim.*

Stochastic Gradient Estimates



Delayed Source Encoding



Avoid storage of forward fields!

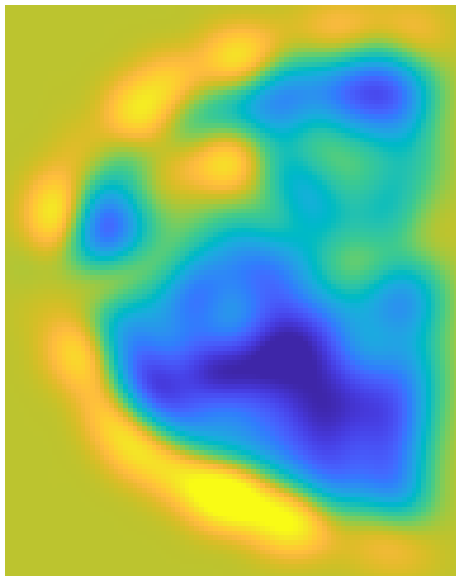
$$(c(x)^{-2}\partial_t^2 - \Delta)p(x, t) = s(x, t), \quad \text{in } \mathbb{R}^d \times [0, T]$$
$$\nabla_c \mathcal{D} = 2 \int_0^T \frac{1}{c(x)^3} \left(\frac{\partial^2 p(x, t)}{\partial t^2} \right) q^*(x, t)$$

Idea: ROI Ω , $\text{supp}(s) \in \Omega^c \times [0, T]$. As $p(x, 0) = p(x, T) = \partial_t p(x, 0) = \partial_t p(x, T) = 0$ in Ω , $p(x, t)$ can be reconstructed from $p(x, t)$ on $\partial\Omega \times [0, T]$ by **time-reversal (TR)**.

- store fwd fields on ROI boundary during forward wave simulation
- interleave backward (adjoint) simulation with TR of boundary data
- 3 instead of 2 wave simulations (unless 2 GPUs used).
- code up efficiently
- multi-layer boundary increases accuracy for pseudospectral method

Multigrid Schemes

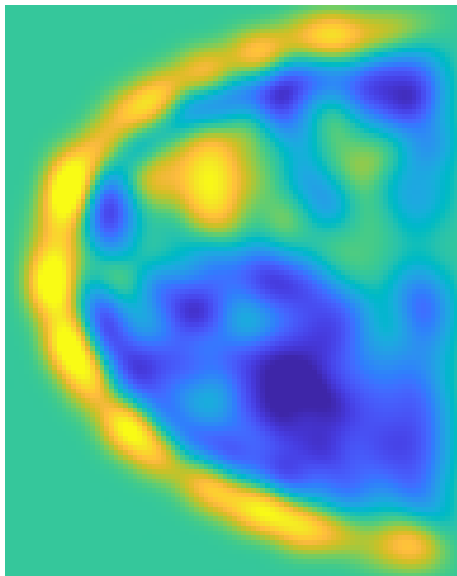
- easy due to regular grids in space and time
- coarsening by 2: (in principle) **speed up of 16**
- most basic multi-grid usage for now: initialization



level 6: upsampled from 5.66mm.

Multigrid Schemes

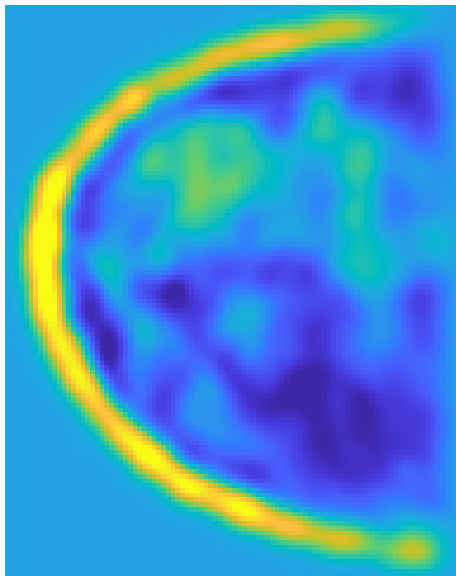
- easy due to regular grids in space and time
- coarsening by 2: (in principle) **speed up of 16**
- most basic multi-grid usage for now: initialization



level 5: upsampled from 4mm.

Multigrid Schemes

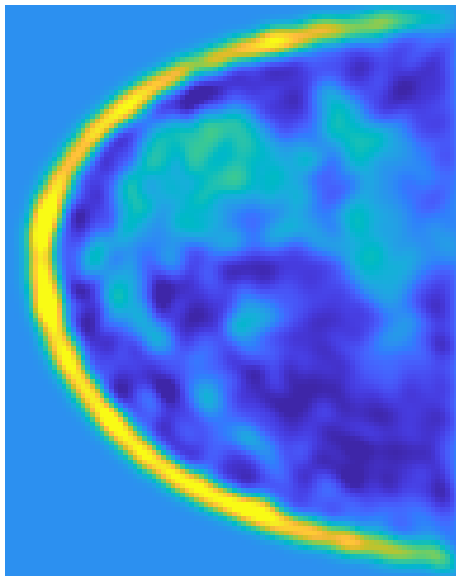
- easy due to regular grids in space and time
- coarsening by 2: (in principle) **speed up of 16**
- most basic multi-grid usage for now: initialization



level 4: upsampled from 2.83mm.

Multigrid Schemes

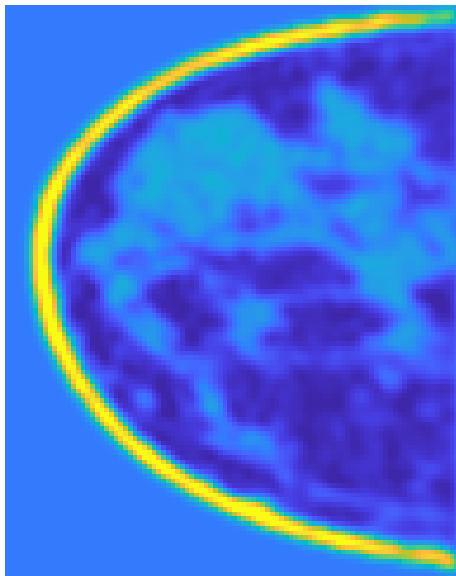
- easy due to regular grids in space and time
- coarsening by 2: (in principle) **speed up of 16**
- most basic multi-grid usage for now: initialization



level 3: upsampled from 2mm.

Multigrid Schemes

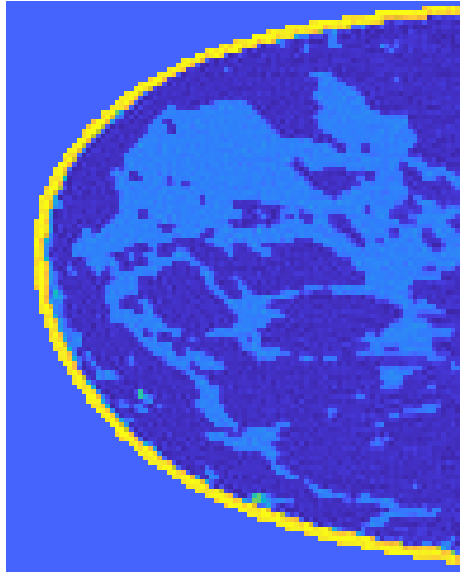
- easy due to regular grids in space and time
- coarsening by 2: (in principle) **speed up of 16**
- most basic multi-grid usage for now: initialization



level 2: upsampled from 1.41mm.

Multigrid Schemes

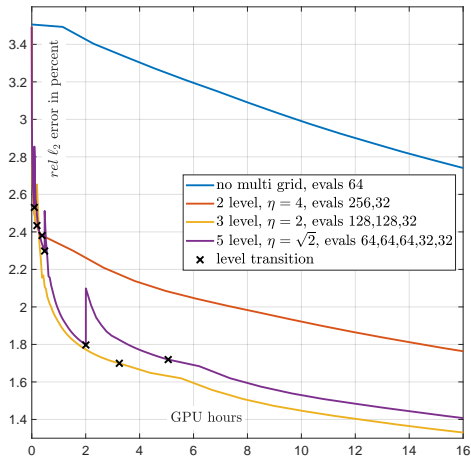
- easy due to regular grids in space and time
- coarsening by 2: (in principle) **speed up of 16**
- most basic multi-grid usage for now: initialization



level 1: resolution 1mm

Multigrid Schemes

- easy due to regular grids in space and time
- coarsening by 2: **speed up of 16** (in principle)
- most basic multi-grid usage for now: initialization



Utilizing Multiple GPUs

- average independent gradient estimates to reduce variance
- not be the best way to use multiple GPUs

